

## Advances in neutral-beam-based diagnostics on the Madison Symmetric Torus reversed-field pinch (invited)

D. J. Den Hartog,<sup>a)</sup> D. Craig, D. A. Ennis, G. Fiksel, S. Gangadhara, D. J. Holly, and J. C. Reardon

*Department of Physics, and Center for Magnetic Self-Organization in Laboratory and Astrophysical Plasmas, University of Wisconsin-Madison, Madison, Wisconsin 53706*

V. I. Davydenko, A. A. Ivanov, and A. A. Lizunov

*Budker Institute of Nuclear Physics, 630090 Novosibirsk, Russia*

M. G. O'Mullane and H. P. Summers

*University of Strathclyde, Glasgow, G1 1XQ Scotland, United Kingdom*

(Received 7 May 2006; presented on 10 May 2006; accepted 31 May 2006; published online 11 October 2006)

Innovative charge-exchange recombination spectroscopy (CHERS), motional Stark effect (MSE), and Rutherford scattering diagnostics are now in operation on the Madison Symmetric Torus (MST) reversed-field pinch (RFP). The CHERS diagnostic measures impurity ion flow and temperature, localized to 2 cm with high time resolution ( $\sim 100$  kHz). A spectral MSE diagnostic has been in use for five years, measuring  $|\mathbf{B}|$  down to 0.2 T with high precision ( $\sim 2\%$ ) and good time resolution (10 kHz). The Rutherford scattering diagnostic has demonstrated the robustness of this technique for reliable measurement of majority (D) ion temperature, also with high time resolution. MST is a large RFP ( $R=1.5$  m,  $a=0.52$  m) operated at moderate current ( $I_p \leq 600$  kA), with  $n_e$  typically  $(1-2) \times 10^{19} \text{ m}^{-3}$  and  $T_e, T_i \leq 2$  keV. Two compact and reliable diagnostic neutral beams are installed on MST. These beams are short pulse, intense, monoenergetic, and low divergence. The first, a neutral H beam, is used in combination with ultraviolet and visible spectroscopy to make the CHERS and MSE measurements. For CHERS, the C VI line at 343.4 nm is collected by a custom high-throughput double grating spectrometer which simultaneously records both charge-exchange and background emissions. The spectrum is analyzed using a sophisticated model derived from the Atomic Database and Analysis Structure (ADAS) package. The MSE system records the entire  $H\alpha$  Stark spectrum;  $|\mathbf{B}|$  is derived from the measured splitting of the  $\pi^+$  and  $\pi^-$  manifolds. Measurement of  $|\mathbf{B}|$  is critical to accurate equilibrium reconstruction in the RFP. The second diagnostic beam is a 20 keV neutral He beam and is used for the Rutherford scattering measurements. A pair of neutral particle analyzers is used to record the energy spectrum of the small-angle Rutherford scattered He atoms. © 2006 American Institute of Physics. [DOI: 10.1063/1.2217920]

### I. INTRODUCTION

Fast dynamics dominate plasma behavior in the Madison Symmetric Torus (MST) reversed-field pinch (RFP). For example, most plasma parameters change dramatically during fast reconnection events (also called “sawtooth crashes”).<sup>1,2</sup> Figure 1 illustrates the rapid increase of magnetic fluctuations, and drop of magnetic energy contained in the plasma, during a fast reconnection event. Typical time scales of interest during these events are 10–100  $\mu\text{s}$ , necessitating diagnostics with a temporal response on the order of 10–100 kHz. Development of a detailed physics understanding requires spatially and temporally resolved measurements of many plasma parameters. In particular, topics such as energy<sup>3</sup> and momentum<sup>4</sup> transport, the magnetohydrodynamic dynamo ( $\tilde{\mathbf{v}} \times \tilde{\mathbf{B}}$ ),<sup>2</sup> and equilibrium reconstruction<sup>5</sup> require plasma temperature, flow, and magnetic field to be precisely measured.

To meet these measurement challenges on MST, we have developed innovative implementations of three diagnostic techniques:<sup>6</sup> charge-exchange recombination spectroscopy (CHERS),<sup>7</sup> Rutherford scattering,<sup>8</sup> and spectral motional Stark effect (MSE).<sup>7</sup> All of these diagnostics are “beam based,” that is, they require injection of a neutral atom beam into the plasma, followed by collection of emitted photons or scattered particles. The characteristics of these diagnostics as implemented on MST are shown in Table I.

Both the CHERS and Rutherford scattering diagnostics measure ion temperature and flow, the former of impurity ions (typically carbon in MST) and the latter of majority ions (deuterium). CHERS has superior spatial resolution, but both diagnostics have high time resolution (100 kHz). This temporal resolution capability is a distinguishing characteristic of the CHERS diagnostic on MST; typically such diagnostics are limited to  $\sim 1$  kHz, although at least one example of a higher-speed implementation has been operated.<sup>9</sup> Besides the requirement for high time resolution, implementation of

<sup>a)</sup>Electronic mail: djdenhar@wisc.edu

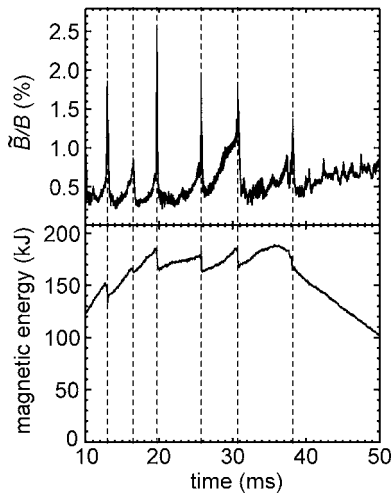


FIG. 1. Reconnection events are marked by dashed lines. The magnetic fluctuation level ( $\tilde{B}/B$ ) and stored magnetic energy both change rapidly during the reconnection events.

CHERS on MST has overcome the specific challenges of both high background light from the plasma and relatively low ion temperature.

Rutherford scattering on MST is a unique diagnostic for several reasons. Currently, there are no other operating Rutherford scattering diagnostics on fusion research devices; most recently the technique has been implemented on a magnetic mirror machine<sup>10</sup> and a tokamak.<sup>11</sup> The implementation on MST has much higher temporal resolution than these previous efforts and is the only Rutherford scattering diagnostic ever implemented on a RFP. Rutherford scattering is one of a small number of diagnostic techniques that directly measures the majority ions in a fusion research plasma; most techniques probe impurity ions, with the implicit assumption that impurity and majority ions are fully equilibrated on all time scales of interest.

The spectral MSE diagnostic on MST measures the magnitude of the magnetic field  $|\mathbf{B}|$  in the center of the plasma. Typical implementations of MSE on high magnetic field ( $|\mathbf{B}| \geq 1$  T) fusion research devices rely on polarimetry of the Stark spectrum to measure the local direction of the magnetic field.<sup>12,13</sup> This technique is difficult to implement at lower fields,<sup>14</sup> so on MST we record the entire motional Stark spectrum and directly measure the component splitting in order to measure  $|\mathbf{B}|$  down to  $\sim 0.2$  T. This measurement of  $|\mathbf{B}|$  is a strong constraint on plasma equilibrium reconstruction.<sup>5</sup>

The advances made in beam-based diagnostics on MST are the result of the implementation of compact, high-brightness diagnostic neutral beams, and the construction of custom high-throughput spectrometers appropriate to the specific diagnostic. Thus, after a brief introduction to the MST RFP, this article is organized as follows: The general characteristics of the neutral beams will be described, then CHERS, Rutherford scattering, and spectral MSE as implemented on MST will be described in separate sections.

## II. THE MST RFP

The RFP can be broadly defined as “toroidal plasma confinement with a low magnetic field.”<sup>15</sup> The toroidal field of a

TABLE I. The characteristics of the beam-based diagnostics implemented on MST.

Diagnostic	Plasma parameters measured	Spatial and temporal resolutions
CHERS	Impurity (C) $T_i$ and $v_i$	2 cm, 100 kHz
Rutherford scattering	Majority (D) $T_i$ and $v_i$	$\sim 14$ cm, 100 kHz
Spectral MSE	$ \mathbf{B}  \geq 0.2$ T, $\sim 2\%$ precision	$\sim 8$ cm, 10 kHz

RFP is typically ten times smaller in a RFP than in a similar plasma current tokamak. Like the tokamak, the RFP is a toroidal magnetic field configuration capable of confining a high-temperature plasma. However, unlike a tokamak where the toroidal magnetic field  $B_\phi$  is much greater than the poloidal magnetic field  $B_\theta$ , in a RFP  $B_\phi \approx B_\theta$ . Furthermore, in a RFP the toroidal magnetic field actually goes to zero and then reverses sign near the edge of the plasma. This magnetic field configuration is produced and sustained by conversion of poloidal flux to toroidal flux inside of a conducting shell, a process often referred to as the “RFP dynamo.”<sup>2</sup> In other words, the magnetic field equilibrium is substantially determined by self-generated plasma currents. The RFP is a “spontaneous” configuration, arising from the “relaxation” of the plasma into a minimum energy state. Internal measurements of the magnetic field in the plasma are critical to equilibrium reconstruction, thus the importance of the spectral MSE diagnostic to measure internal  $|\mathbf{B}|$ .

MST is a large RFP with major radius  $R=1.5$  m, minor radius  $a=0.5$  m, and a thick (5 cm) aluminum conducting shell.<sup>16</sup> The aluminum conducting shell, in addition to serving as vacuum vessel, is the one-turn toroidal field coil. This means that diagnostic port access through the vacuum vessel is not hampered by large discrete toroidal field coils. Instead, diagnostic port access is strictly limited by the fact that large currents flow in the aluminum vessel, thus port size is restricted in order to minimize disruption of these currents. For example, the neutral beam used for CHERS is injected through a 5 cm diameter port, and the CHERS signal is collected through ports of the same diameter.

Typical plasma parameter ranges in MST are toroidal plasma current  $I_p$  between 0.2 and 0.6 MA,  $|\mathbf{B}| \leq 0.5$  T, electron density  $n_e$  between 0.5 and  $2.5 \times 10^{13}$  cm<sup>-3</sup>, and electron  $T_e$  and ion  $T_i$  temperatures between 50 and 2000 eV. A typical plasma discharge is approximately 70 ms in duration, with a 20–30 ms “flat top” in which the plasma current is nearly constant and the plasma is roughly in equilibrium. Over 100 plasma discharges are often produced during a day of MST operation in order to collect large ensembles of data. Shot-to-shot reproducibility is good, enabling statistical uncertainty to be reduced by ensemble averaging measurements of fast reconnection events.<sup>2</sup> Diagnostics must be able to match a cycle in which data are collected at high rates for  $\sim 30$  ms every 2–4 min.

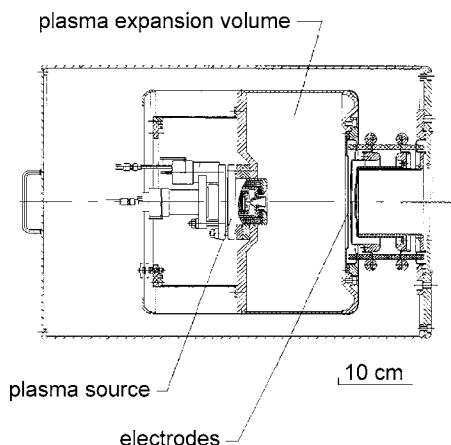


FIG. 2. Cross-sectional view of the diagnostic neutral beam injector.

### III. DIAGNOSTIC NEUTRAL BEAMS

Two compact and reliable diagnostic neutral beams are installed on MST. These beams were constructed by the Budker Institute of Nuclear Physics in Novosibirsk, Russia and are the result of decades of development and improvement.<sup>17</sup> On MST, a hydrogen (H) beam with 50 keV atom energy is used for CHERS and MSE. This beam has a 20 ms pulse duration, well matched to the MST discharge flat top. It is a replacement and upgrade for a 30 keV, 3 ms pulse H beam that functioned extremely reliably for several years. CHERS and MSE results contained in this article were taken with both beams; differentiation is not made. The second beam on MST is a 20 keV, 3 ms pulse helium (He) beam used for Rutherford scattering. The common characteristics shared by the beams are low beam divergence ( $\sim 15$  millirad), mono-species ( $>90\%$  of the beam atoms are at the full energy), and monoenergetic (beam atom energy spread  $<1\%$  of the full energy). These characteristics greatly simplify the implementation of CHERS and Rutherford scattering and are crucial to the successful operation of the spectral MSE diagnostic.

Neither beam produces a significant perturbation of the plasma in MST, as the absorbed beam power is typically a few percent of the several megawatts of Ohmic input power.

Each beam injector contains an ion source in which ions are extracted from a dense plasma created by a miniature arc discharge source (Fig. 2). The plasma from the source is allowed to expand into a large volume; this reduces its perpendicular temperature, thus enabling achievement of low beam divergence. The extracted ion beam is accelerated and focused by a compact ion optical system and neutralized by passing through a gas cell. The H beam as installed on MST is shown in Fig. 3.

### IV. CHERS

To date, the most successful tool for localized impurity ion measurements in fusion research plasmas is CHERS.<sup>18,19</sup> CHERS is a two-step process:  $H^0 + A^{+Z} \rightarrow H^+ + A^{+(Z-1)}(n, l) \rightarrow A^{+(Z-1)}(n', l') + h\nu$ . In the first step, a neutral hydrogen atom  $H^0$  is injected into the plasma by a high-energy beam and charge exchanges with a (usually) fully ionized intrinsic impurity  $A^{+Z}$  such as He, C, or O. The charge-exchange pro-

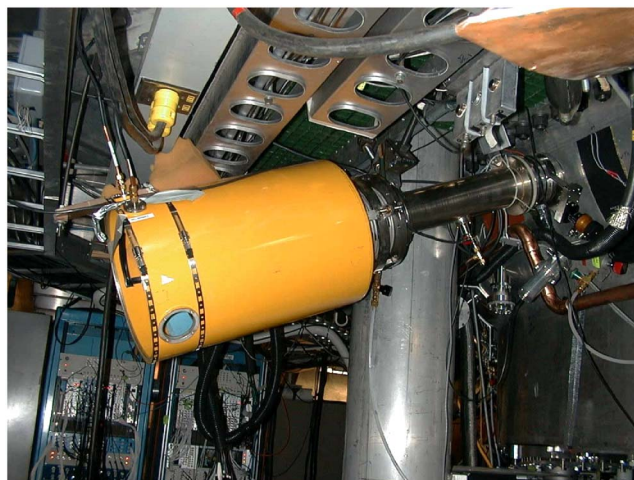


FIG. 3. (Color online) Side view of the 30 keV hydrogen neutral beam injector as installed on MST.

cess typically leaves the impurity  $A^{+(Z-1)}$  in some excited state  $(n, l)$ , which then radiatively decays, emitting a photon  $h\nu$ . The wavelength of this photon is Doppler shifted from the line emission center by the thermal and directed kinetic motions of the impurity ion. Recording the Doppler-broadened emission spectrum with an appropriate spectrometer allows determination of the impurity ion temperature from the width of the spectrum and the directed flow velocity of the impurity ion from the absolute shift of the line emission center.

We conducted an extensive survey of ultraviolet and visible transitions in MST to find an appropriate candidate for CHERS measurements.<sup>7</sup> The C VI transition at 343.369 nm is relatively strong, gives the largest charge-exchange signal/background ratio of any line surveyed, and is reasonably well isolated in MST. “Contamination” due to O VI emission at 343.3 nm exists but is not a severe problem.

Although the C VI emission from charge exchange with the beam is strong, the background signal from the plasma is of the same order or larger in most circumstances. High background neutral density in MST results in substantial charge exchange of  $C^{+6}$  with thermal neutrals in the plasma; the  $C^{+5}$  ions thus created are excited by electron impact, and decay producing substantial background emission at the C VI transition of interest. In order to distinguish between beam-induced and background emissions, we have implemented a dynamic background measurement technique with two optical views through each viewing port: one intersecting the beam and one to the side. Figure 4 illustrates the implementation of this technique. The neutral beam is shown being injected perpendicular to the plane of the figure. The “beam view” intersects the beam, recording both beam and background emissions, while the “background view” is  $\sim 2$  cm offset in the toroidal direction and does not intersect the beam. The position of the background view has been carefully adjusted so that it is as close as possible to the beam, yet does not collect charge-exchange emission. Collection of light from these two chords with the beam off indicates that the background emission recorded by both is nearly identical.

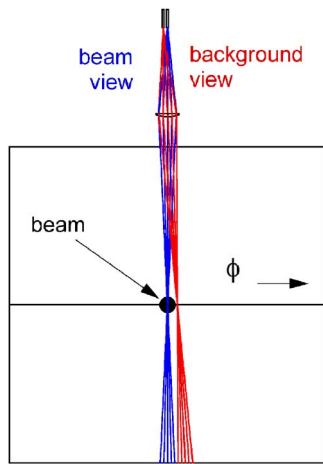


FIG. 4. (Color online) CHERS measurements are made in MST with two optical views through each viewing port: one intersecting the beam and one to the side. The “beam view” intersects the beam, while the “background view” is  $\sim 2$  cm offset in the toroidal direction and does not intersect the beam.

CHERS measurements can be made at eleven radial points on a poloidal cross section of MST (Fig. 5). The optical views are perpendicular to the neutral beam. This maximizes radial spatial resolution ( $\sim 2$  cm), as the magnetic flux surfaces in the plasma are also perpendicular to the beam. Since only one high-throughput CHERS spectrometer has been built for use on MST, data are collected from one radial point at a time. However, a full radial profile of impurity ion temperature,  $T_i(r)$ , can be collected in a single day of MST operation by moving the viewing fiber bundles from port to port. A planned upgrade is the construction of several more high-throughput CHERS spectrometers in order to obtain real-time profile information.

The custom high-throughput CHERS spectrometer is the key to measuring fast impurity ion dynamics in MST and is described in detail in Ref. 20. This spectrometer was completely designed and constructed in our laboratory. It is actually a *duo*-spectrometer, as it simultaneously records emission from both the beam and background views. Two separate fiber bundles transport light from the viewing port to the curved entrance slit, where one view fills the upper half of the slit, and the other view, the bottom half. The light is dispersed by two gratings in a Czerny-Turner layout.<sup>21</sup> This double grating design is required to obtain the dispersion necessary to allow wide slits, which in turn are necessary to obtain the étendue required to provide high throughput. The spectra at the exit plane of the spectrometer are dispersed onto columns of fiber optics, each column sampling a small  $\Delta\lambda$  wavelength band of either the beam view or background view spectrum. Each column of fiber optics transports light to a photomultiplier tube, from which the signal is amplified and digitized by an independent digitizer channel. Each spectrum is dispersed onto 16 wavelength channels.

For CHERS analysis, the emission line shapes are modeled using Atomic Data and Analysis Structure (ADAS).<sup>22</sup> Both the beam-driven charge-exchange and background electron-impact emissions are modeled.<sup>23</sup> Since the ion tem-

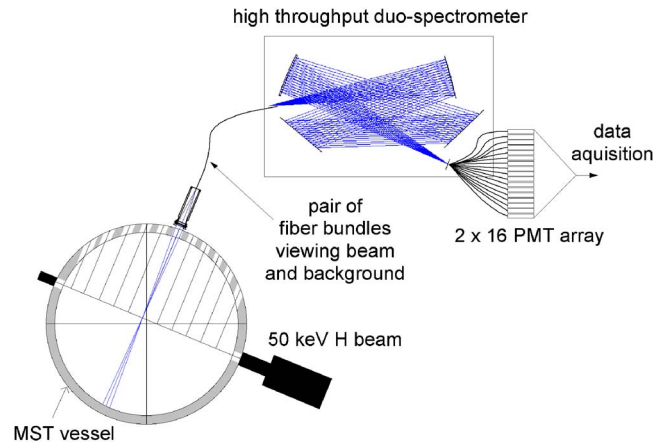


FIG. 5. (Color online) Poloidal cross section of MST, showing the eleven radial points for CHERS measurements. The H beam is injected radially across the plasma at  $22.5^\circ$  below the midplane of MST.

perature in MST is relatively low, the thermal Doppler broadening of the C VI line at 343.369 nm is not substantially larger than the separation of the fine-structure components of this transition. Thus the amplitude and separation of these components are modeled with ADAS and the Doppler-broadened sum calculated for both charge-exchange and electron-impact emissions of the C VI line. The contribution to background emission by O VI line emission is also modeled.

The beam-driven charge-exchange signal is derived from coupled fits of both background (from the background view) and total (from the beam view) emissions. The background contains only electron-impact emission, while the total emission has both the charge-exchange signal and electron-impact emissions. Direct subtraction of the background from the total emission, and then a fit of the remainder, is not as effective as coupled fits of each individually. The beam-driven charge-exchange spectrum provides localized measurement of the impurity flow and temperature.

## V. RUTHERFORD SCATTERING

In a plasma diagnostics context, Rutherford scattering refers to the small-angle nuclear scattering of injected beam atoms by plasma ions. This small-angle Coulomb scattering process is basically mechanical, conserving energy and momentum. If the injected beam is monoenergetic, the energy distribution of the scattered atoms is determined by the velocity distribution of the ions. Thus, the ion temperature is determined from the measured width of the scattered atom energy distribution and the ion flow velocity from the shift of the energy spectrum. In the simplest case, a monoenergetic beam (of energy  $E_0$ ) with zero angular spread, the energy spectrum of atoms scattered by an angle  $\theta \ll 1$  is approximately Gaussian, with a variance  $\Delta = \sqrt{2\mu E_0 T_i} \theta^2$  and centroid  $E_c = E_0(1 - \mu\theta^2)$ , where  $\mu = m_b/m_i$ ;  $m_b$  is the mass of the beam atoms and  $m_i$  the mass of the majority ions in the plasma. There is an additional shift in  $E_c$  caused by nonzero majority ion flow velocity, not included in this simple equation. On MST,  $\theta$  is chosen to be about  $10^\circ$  as a compromise between improved accuracy and decreased signal (due to the

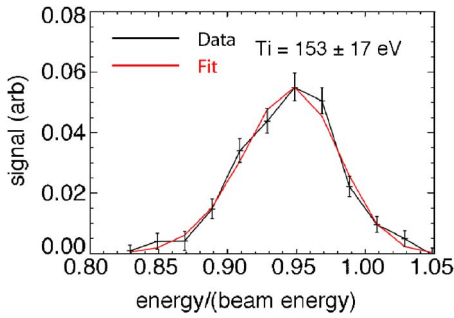


FIG. 6. (Color online) A typical Rutherford scattering energy spectrum from MST, collected over a 10  $\mu\text{s}$  time window.

well-known  $1/\sin^4\theta$  dependence of the Rutherford scattering cross section). A complication arises for a real beam with nonzero energy spread and angular divergence, since in this case a detector at a fixed location observes atoms which have undergone scattering by a range of angles  $\theta$ . The  $\theta$  dependence in the scattering cross section then results in a non-Gaussian spectrum. In addition, a real energy analyzer with a finite acceptance angle will record scatterings which have occurred over a finite volume, again with a range of  $\theta$ . Nevertheless, a typical Rutherford scattering spectrum is recognizably Gaussian (Fig. 6) and is well fit by the type of model described in Ref. 8.

In MST, a 20 keV beam of He atoms is used for Rutherford scattering. A He beam was chosen because of the high ionization threshold of He; the beam penetrates well into the plasma and, once scattered, the He atom is likely to reach the detector rather than be lost to ionization. The scattered He atom energy spectrum also has reasonable width and good shift of  $E_c$  from the beam energy. The scattered atoms are detected by two 12-channel electrostatic energy analyzers,<sup>8</sup> which were designed and constructed by the Budker Institute. A cross-sectional view of the entire Rutherford scattering diagnostic installation on MST is shown in Fig. 7. The axes of the two analyzers can be tilted or translated indepen-

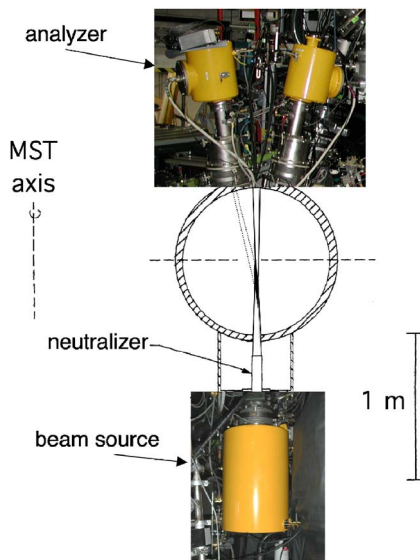


FIG. 7. (Color online) Cross-sectional view of the Rutherford scattering diagnostic on MST.

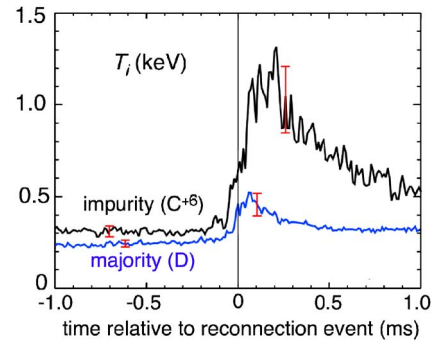


FIG. 8. (Color online) Ensemble average of majority and impurity ion temperature during a fast reconnection event in MST.

dently and can acquire spectra from two spatial points. A profile can be acquired by tilting an analyzer between shots, although typical operation is with the center of the beam and analyzer sight line at  $r/a \cong 0.35$ . Resulting radial resolution is  $\sim 14$  cm.

Rutherford scattering and CHERS are complementary diagnostics in several respects. CHERS has very good spatial resolution ( $\sim 2$  cm) while Rutherford scattering is somewhat coarse. Rutherford scattering, however, measures majority ion properties while CHERS typically measures impurity ions. Both have excellent temporal resolution on MST. The ability to make both measurements simultaneously enables direct comparison of the rapid heating of ions that occurs during a fast reconnection event (Fig. 8). Both majority and impurity temperatures increase dramatically on time scales of 100  $\mu\text{s}$ , but the majority increase is substantially less than the impurity. This implies a charge or mass dependence to the heating mechanism and is valuable input to theoretical models of ion heating in the RFP.

## VI. SPECTRAL MSE

In many low-field ( $< 0.5$  T) fusion research devices such as reversed-field pinches, magnetic mirrors, and spherical tori, the magnitude of the magnetic field in the core of the plasma is an important constraint for equilibrium modeling. In these devices the vacuum magnetic field profile can be greatly altered by dynamo, diamagnetic, or other plasma driven mechanisms. In order to measure internal  $|\mathbf{B}|$  in MST, we have implemented a spectral MSE diagnostic.<sup>24</sup> Similar diagnostics have been installed on a tokamak<sup>25</sup> and a magnetic mirror.<sup>26</sup> This diagnostic requires a direct measurement of the entire Balmer- $\alpha$  motional Stark spectrum emitted by the neutral hydrogen beam atoms injected into the plasma. The beam atoms are excited by collisions with the plasma (primarily electrons), and the beam atom electron energy levels are Stark split by the motional electric field  $\mathbf{E} = \mathbf{v}_{\text{beam}} \times \mathbf{B}$ , where  $\mathbf{v}_{\text{beam}}$  is the directed velocity of the beam and  $\mathbf{B}$  is the local magnetic field in the plasma. On MST, we measure the separation of the  $\pi$  manifolds of the Stark-split Balmer- $\alpha$  line at 656.3 nm. This splitting is typically 0.2 nm or less for most plasma discharges in MST. Since the beam velocity is accurately known, the measured separation is directly analyzed to extract local  $|\mathbf{B}|$ .

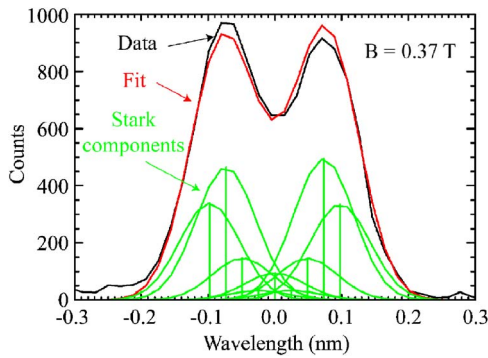


FIG. 9. (Color online) Typical spectral MSE spectrum from MST, showing data, fit, and the individual Stark components of the fit.

MSE is a relatively common tool for making internal magnetic field measurements in high-field ( $|\mathbf{B}| \geq 1$  T) plasmas. The motional Stark manifold is composed of  $\pi$  transitions (polarized parallel to the motional  $\mathbf{E}$ ) and  $\sigma$  transitions (polarized perpendicular to the motional  $\mathbf{E}$ ). For high-field fusion research devices with energetic neutral beams, the motional  $\mathbf{E}$  is large ( $\sim 10$  MV/m) and the  $\pi$  and  $\sigma$  components are spectrally isolated. Thus, some form of polarimetry can be used to obtain information on the magnetic field direction and magnitude. This works well provided the different polarization components do not overlap in wavelength space. This is generally not the case for low-field devices such as the RFP.<sup>27</sup> The individual components of the Stark manifold are broadened primarily by these effects: a beam which is not completely monoenergetic, finite beam divergence, and finite light collection volume. Deviations from a monoenergetic beam can be characterized by a finite parallel temperature of the beam atoms, while a finite perpendicular temperature of the beam atoms contributes to beam divergence. A finite perpendicular temperature can arise from perpendicular thermal energy of beam atoms and/or from geometric focusing by the ion optics. A finite light collection volume for beam emission requires a spread of observation angles, resulting in varying Doppler shifts for the collected beam emission photons. On MST, low beam temperatures and carefully designed optics resulted in a total line smearing of full width at half maximum (FWHM)  $\approx 0.1$  nm for spectral MSE operation with the 30 keV H beam. With the 50 keV H beam, the smearing is currently greater than 0.1 nm, but the beam will be upgraded in the next year to reduce the beam divergence. This may allow the MSE diagnostic on MST to measure fields below 0.2 T, as the higher energy of this beam produces greater wavelength separation of the motional Stark manifold at a given magnetic field.

An alternative method for MSE measurement at low field is to reduce the effect of beam divergence and collection angles by effectively collimating the beam with laser induced fluorescence (LIF).<sup>28,29</sup> In combination with a nearly monoenergetic beam, this technique may enable MSE measurement at very low fields.

Figure 9 shows a typical Stark spectrum from MST. Each of the individual Stark components is fit as a Gaussian-broadened line with the relative amplitudes of the components fixed and set by a model assuming statistical popula-

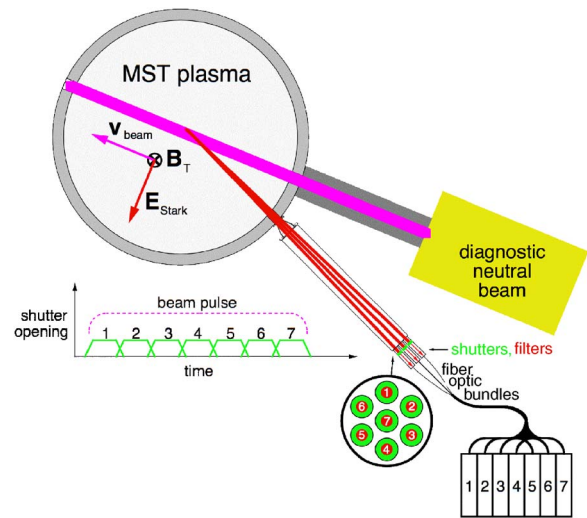


FIG. 10. (Color online) An illustration of the spectral MSE diagnostic on MST. Seven views through individual FLC shutters and optical bandpass filters are each mapped to an individual slit on the CCD spectrometer. For clarity, some details are not shown in this illustration; for example, space limitations constrained all but the central view of the hexagonal pack to be bent through  $90^\circ$  prior to the collection telescopes containing the shutters and filters.

tion of the excited levels.<sup>30</sup> The fit model is  $C \sum_i a_i \exp[-(\lambda - \lambda_i)^2 / 2\Delta\lambda^2]$ , where  $C$ ,  $\lambda_i$ , and  $\Delta\lambda$  are the fitted parameters. The amplitudes and wavelengths of the Stark components are  $a_i$  and  $\lambda_i$ , respectively, and  $\Delta\lambda$  is the component broadening. From the component separation local  $|\mathbf{B}|$  is derived to approximately 2% precision, with uncertainty determined primarily by photon statistics. Additional improvements in the accuracy of the measurement await further development of an atomic model for analysis of MSE data. This model will be a part of ADAS and will include both the Stark and Zeeman effects, fine structure, and a collisional-mixing population model. In particular, it is hoped that this model will fit the amplitude asymmetry apparent in the  $\pi^+$  and  $\pi^-$  manifolds (Fig. 9). This asymmetry is persistent in MSE data from MST and does not appear to be an experimental artifact.

An illustration of the spectral MSE diagnostic on MST is shown in Fig. 10. The neutral beam is the same one used for CHERS. Beam emission is collected with viewing chords at an angle of  $22.5^\circ$  to the beam axis, thus the Balmer- $\alpha$  beam emission is Doppler shifted several nanometers away from the background thermal Balmer- $\alpha$  emission from the plasma. The chords intersect the beam at the approximate magnetic axis of MST, which is shifted  $\sim 6$  cm from the geometric axis.<sup>5</sup> Seven individual viewing telescopes are arranged in a hexagonal array. Inside each telescope is a Displaytech ferroelectric liquid crystal (FLC) shutter, and all telescopes but the central include a custom bandpass optical interference filter (Andover Corporation) centered on the Doppler-shifted Balmer- $\alpha$  beam emission. The FLC shutter is intrinsically a linear polarizer and is adjusted to pass vertical polarization so that primarily the  $\pi$  components are recorded from the beam emission. Light from each of the views is fiber optically mapped onto an individual full-height entrance slit on the spectrometer. In other words, there are seven full-height

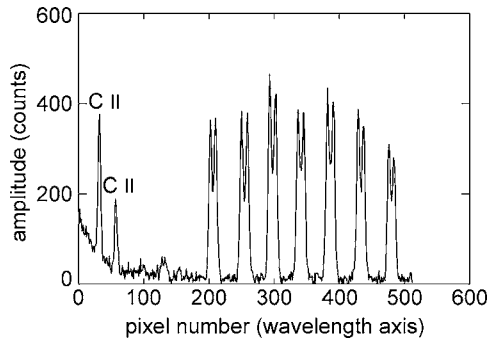


FIG. 11. Seven independent MSE spectra are recorded on each frame of the CCD camera.

entrance slits on the entrance plane of the spectrometer, each slit slightly horizontally displaced from the other. This arrangement enables each viewing chord to take advantage of the full étendue available from the spectrometer. The band-pass filters on six of chords prevent spectral overlap; the remaining chord passes two C II lines that provide *in situ* wavelength calibration of the spectrometer (Fig. 11).

The spectrometer is based on a commercial  $f/6.5$ , 0.5 m Czerny-Turner (Acton Research Corp.) with an 1800 g/mm grating. The seven rectangular entrance slits (each  $0.020 \times 14 \text{ mm}^2$  with a pitch of 0.864 mm) were etched into a mask of 0.0005 in. thick stainless steel shim stock (PCM Products, Inc.). This mask is mounted in an alignment fixture that replaces the stock entrance slit assembly of the spectrometer. The fiber optic bundle butted directly to the seven entrance slits is illustrated in Fig. 12. The fibers are filled at approximately  $f/6$  by the viewing telescopes, and thus slightly overfill the spectrometer (the fibers preserve the  $f/\#$  of the input cone of light). The detector is a charge-coupled device (CCD) camera (Princeton Instruments, Inc.). This camera has slow frame readout in order to obtain very low read noise. As a consequence, only one camera frame (with seven MSE spectra, Fig. 11) is obtained from every MST discharge. The FLC shutters are triggered sequentially during the CCD exposure, typically with individual shutter times of 100–300  $\mu\text{s}$ . This provides a short measurement sequence of

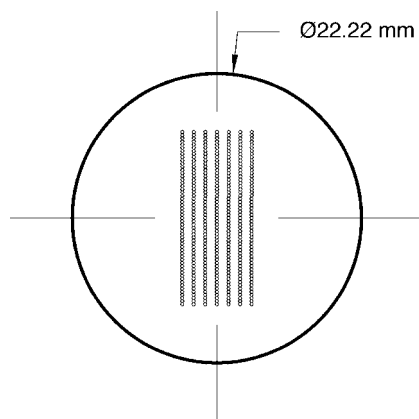


FIG. 12. The face of the fiber optic bundle butted to the seven entrance slits of the spectrometer. Each column is 55 fibers, fused silica, 200  $\mu\text{m}$  core/220  $\mu\text{m}$  clad/245  $\mu\text{m}$  jacket. Each column is filled with light collected by an individual viewing telescope.

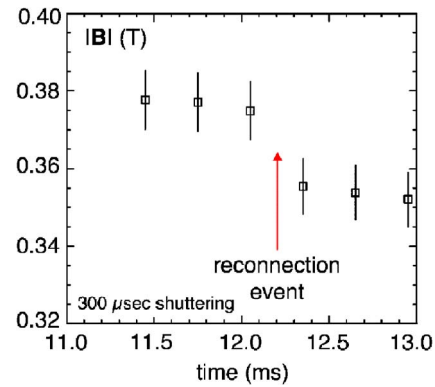


FIG. 13. Spectral MSE measurement of  $|\mathbf{B}|$  for a single reconnection event in MST, using 300  $\mu\text{s}$  shutter times.

$|\mathbf{B}|$  time development in the plasma (Fig. 13). For increased detail, an ensemble average of such events is acquired (Fig. 14). Note the expanded vertical scale of these graphs; relative changes of 0.01 T in  $|\mathbf{B}|$  are easily measured.

Further development of the spectral MSE diagnostic on MST is in progress on two fronts. First, the CCD camera currently in use is being replaced with an electron-multiplying CCD camera (Princeton Instruments, Inc.). This camera has the possibility to record a complete frame every 1–2 ms, with very low read noise. This mode of operation will allow all seven FLC shutters to be fired during each frame, producing repeated sequences of  $|\mathbf{B}|$  time development throughout the 20 ms neutral beam pulse duration. This will enable much faster collection of data ensembles and provide nearly continuous recording of MST equilibrium evolution during the flat-top portion of a discharge. The second development in progress is the addition of another set of chords viewing a half-radius point in the plasma. Unlike the view of the MST magnetic axis, where  $\mathbf{B}$  is completely toroidal,  $\mathbf{B}$  at this point is a mixture of toroidal and poloidal directions. Thus both vertically and horizontally polarized beam emissions will be collected in order to enable accurate fits of the Stark spectrum and determination of the direction of  $\mathbf{B}$ .

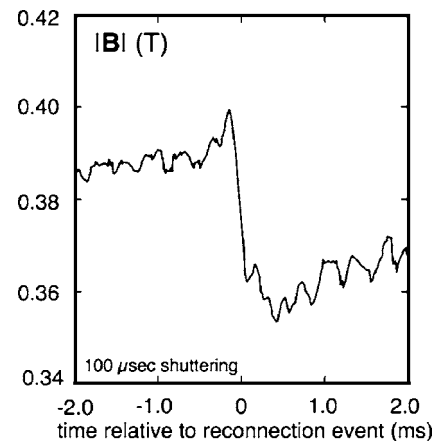


FIG. 14. Spectral MSE measurement of  $|\mathbf{B}|$  for an ensemble of reconnection events in MST, using 100  $\mu\text{s}$  shutter times.

## VII. SUMMARY

Advanced CHERS, Rutherford scattering, and MSE diagnostics are routinely operated on MST to measure fast plasma dynamics. We have pursued a two-pronged approach to advancing beam-based diagnostics and overcoming the specific challenges of diagnostic implementation on MST. First, compact, high-brightness diagnostic neutral beams provide the necessary low beam divergence and monoenergetic atoms. Second, custom high-throughput spectrometers record sufficient emitted light (or sufficient scattered atoms) to enable precise high-speed internal measurement of ion temperature and flow, and magnetic field. New physics (some unexpected) has already been obtained, e.g., that impurity and majority ion heating differ during a fast reconnection event.

## ACKNOWLEDGMENTS

The authors wish to acknowledge the contributions of the entire MST group, both scientific and technical staff, to the successful implementation and operation of these beam-based diagnostics. This work is supported by the U. S. Department of Energy, the National Science Foundation, and the U. S. Civilian Research and Development Foundation.

<sup>1</sup>S. Hokin *et al.*, *Phys. Fluids B* **3**, 2241 (1991).

<sup>2</sup>D. J. Den Hartog, J. T. Chapman, D. Craig, G. Fiksel, P. W. Fontana, S. C. Prager, and J. S. Sarff, *Phys. Plasmas* **6**, 1813 (1999).

<sup>3</sup>T. M. Biewer *et al.*, *Phys. Rev. Lett.* **91**, 045004 (2003).

<sup>4</sup>A. K. Hansen, A. F. Almagri, D. Craig, D. J. Den Hartog, C. C. Hegna, S. C. Prager, and J. S. Sarff, *Phys. Rev. Lett.* **85**, 3408 (2000).

<sup>5</sup>J. K. Anderson, C. B. Forest, T. M. Biewer, J. S. Sarff, and J. C. Wright, *Nucl. Fusion* **44**, 162 (2004).

<sup>6</sup>D. J. Den Hartog, D. Craig, G. Fiksel, J. C. Reardon, V. I. Davydenko, and A. A. Ivanov, in *Advanced Diagnostics for Magnetic and Inertial Fusion*, edited by Peter E. Stott *et al.*, (Kluwer Academic, Dordrecht/Plenum, New

York, 2002), pp. 237–240.

<sup>7</sup>D. Craig, D. J. Den Hartog, G. Fiksel, V. I. Davydenko, and A. A. Ivanov, *Rev. Sci. Instrum.* **72**, 1008 (2001).

<sup>8</sup>J. C. Reardon *et al.*, *Rev. Sci. Instrum.* **72**, 598 (2001).

<sup>9</sup>H. T. Evensen, R. J. Fonck, S. F. Paul, G. Rewoldt, S. D. Scott, W. M. Tang, and M. C. Zarnstorff, *Nucl. Fusion* **38**, 237 (1998).

<sup>10</sup>A. A. Zuev, A. A. Ivanov, A. N. Karpushov, E. Yu. Kolesnikov, S. V. Murakhtin, and S. L. Strogalova, *Plasma Phys. Rep.* **28**, 268 (2002).

<sup>11</sup>H. F. Tammen, A. J. Donné, T. Oyevaar, and F. C. Schüller, *Plasma Phys. Rep.* **20**, 158 (1994).

<sup>12</sup>A. Boileau, M. von Hellermann, W. Mandl, H. Weisen, and A. Zinoviev, *J. Phys. B* **22**, L145 (1989).

<sup>13</sup>F. M. Levinton, R. J. Fonck, G. M. Gammel, R. Kaita, H. W. Kugel, E. T. Powell, and D. W. Roberts, *Phys. Rev. Lett.* **63**, 2060 (1989).

<sup>14</sup>F. M. Levinton, *Rev. Sci. Instrum.* **70**, 810 (1999).

<sup>15</sup>S. Ortolani and D. D. Schnack, *Magnetohydrodynamics of Plasma Relaxation* (World Scientific, Singapore, 1993).

<sup>16</sup>R. N. Dexter, D. W. Kerst, T. W. Lovell, S. C. Prager, and J. C. Sprott, *Fusion Technol.* **19**, 131 (1991).

<sup>17</sup>G. F. Abdrashitov *et al.*, *Rev. Sci. Instrum.* **72**, 594 (2001).

<sup>18</sup>R. J. Fonck, D. S. Darrow, and K. P. Jaehnig, *Phys. Rev. A* **29**, 29 (1984).

<sup>19</sup>R. C. Isler, *Plasma Phys. Controlled Fusion* **36**, 171 (1994).

<sup>20</sup>D. Craig, D. J. Den Hartog, D. A. Ennis, S. Gangadhara, and D. Holly, *Rev. Sci. Instrum.* (submitted).

<sup>21</sup>M. V. R. K. Murty, *Opt. Eng. (Bellingham)* **13**, 23 (1974).

<sup>22</sup>The original developer of ADAS is the JET Joint Undertaking; <http://adas.phys.strath.ac.uk/>

<sup>23</sup>S. Gangadhara, D. Craig, D. A. Ennis, and D. J. Den Hartog, *Rev. Sci. Instrum.* these proceedings.

<sup>24</sup>D. J. Den Hartog, D. Craig, G. Fiksel, V. I. Davydenko, A. A. Ivanov, and A. A. Lizunov, Third Plasma Polarization Spectroscopy Workshop, Livermore, CA, 2001 [Lawrence Livermore National Laboratory Report No. UCRL-ID-146907 (unpublished)], pp. 205–208.

<sup>25</sup>R. Jaspers, B. S. Q. Elzendoorn, A. J. H. Donné, and T. Soetens, *Rev. Sci. Instrum.* **72**, 1018 (2001).

<sup>26</sup>P. A. Bagryansky *et al.*, *Rev. Sci. Instrum.* **74**, 1592 (2003).

<sup>27</sup>L. Carraro, M. E. Puiatti, F. Sattin, P. Scarin, and M. Valisa, *Rev. Sci. Instrum.* **70**, 861 (1999).

<sup>28</sup>E. L. Foley and F. M. Levinton, *Rev. Sci. Instrum.* **75**, 3462 (2004).

<sup>29</sup>E. L. Foley and F. M. Levinton, *Rev. Sci. Instrum.* these proceedings.

<sup>30</sup>W. Mandl, R. C. Wolf, M. G. von Hellermann, and H. P. Summers, *Plasma Phys. Controlled Fusion* **35**, 1373 (1993).